Dependence of solar reflector soiling on location relative to a ferromanganese smelter

M.A. Swart[1,2], L. Hockaday[3], Q.G. Reynolds[1,4], and K.J. Craig[2]

Affiliation:
[1]Pyrometallurgy Division, Mintek, South Africa.
[2]Department of Mechanical and Aeronautical Engineering, University of Pretoria, South Africa.
[3]Western Australia School of Mines, Curtin University, Australia.
[4]Department of Chemical Engineering, Stellenbosch University, South Africa.

Correspondence to:
M.A. Swart

Email:
u04535465@tuks.co.za

Dates:
Received: 10 Feb. 2022
Revised: 8 Dec. 2022
Accepted: 8 Dec. 2022
Published: June 2023

How to cite:
Swart, M.A., Hockaday, L., Reynolds, Q.G, and Craig, K.J. 2023
Dependence of solar reflector soiling on location relative to a ferromanganese smelter.
Journal of the Southern African Institute of Mining and Metallurgy, vol. 123, no. 6. pp. 299-308

DOI ID:
http://dx.doi.org/10.17159/2411-9717/2021/2023

ORCID:
M.A. Swart
http://orcid.org/0000-0002-5145-6273
L. Hockaday
http://orcid.org/0000-0003-2597-9756

Synopsis

A solar reflector soiling study was carried out at a ferromanganese smelter in South Africa to assess the soiling rates at different locations around the plant. Several meteorological parameters were monitored to give insight into the conditions that lead to increased soiling. Mineralogical characterization of dust samples collected from the reflectors and the atmosphere revealed that only a certain size fraction is of importance with regard to soiling, and that the dust can be attributed to both raw materials and smelter products. Proximity to the dust source was the primary driver for increased soiling. The site that experienced the most soiling was very close to raw material heaps; this was deemed an outlier and was excluded from the summary statistics. The secondary driver for increased soiling was location relative to the smelter dust sources and the wind's direction and speed. The reflector set at the best location experienced 13.1% less soiling than the set at the 'worst' (but still feasible) location, represented by an averaged mean daily reflectance loss of 0.0186. The study revealed that while there are periods of intense soiling at this particular site, proper planning of reflector location in relation to the smelter dust sources can significantly mitigate the soiling rate.

Keywords

Heliostat soiling, energy-intensive industry (EII), solar thermal process heat, concentrating solar thermal (CST).

Introduction

Energy-intensive industries (EIIs) are major carbon emission sources, consuming a large portion of global energy and emitting roughly a third of global greenhouse-gases (IPCC, 2014). Some mineral processing activities, such as smelting, are major carbon emitters and the demand for the products is likely to increase (Hund *et al.*, 2020). The successful integration of concentrating solar thermal (CST) technologies with EIIs is set to lessen their reliance on fossil fuels and their impact on the climate. The performance of a concentrating solar (CS) plant depends largely on the optical performance of its reflectors, but the effects of industrially generated dust on the performance of solar reflectors are still largely unknown.

Solar photovoltaic (PV) and other renewables that generate power have been developed extensively and are quite mature (IRENA, 2021), but renewable technologies that provide high-temperature (> 600°C) thermal process heat directly are in need of further development. Low-temperature (< 400°C) solar process heat has been used industrially for some time (Weiss and Spörk-Dür, 2021), but only recently have technologies able to supply higher temperature solar process heat started moving closer to commercialization (Ebert *et al.*, 2018).

There are various challenges associated with integrating solar process heat into EIIs. These include industry readiness, energy conversion technology readiness, continuity of heat supply, ease of process adaptation, unknowns regarding process responses to the introduction of solar energy stream, unknowns around CST system performance, and economic feasibility. These challenges are in addition to those that need to be addressed for typical concentrating solar power (CSP) installations, where optimal operation is not yet always achieved (Mehos *et al.*, 2020).

Research is under way towards addressing these challenges, for example the work of Reichart *et al.* (2021) on a novel high-temperature gas-particle heat exchanger to exchange solar process heat stored in particles with air for introduction into an EII process stream. The system-side response to the introduction of solar process heat is also being investigated (Sambo, Hockaday, and Seodigeng, 2020). Mckechnie, McGregor, and Venter (2020) modelled the CST system requirements to feed thermal energy to a manganese ferroalloy smelting plant that processes 40 t of ore per hour, and the financial feasibility of such an integration (Hockaday *et al.*, 2020).

Dependence of solar reflector soiling on location relative to a ferromanganese smelter

An area of CS and PV research that has been receiving increased attention is soiling of solar panels and reflectors (Costa, Diniz, and Kazmerski, 2016, 2018; Kazmerski, Diniz, and Costa, 2020). The performance of a PV cell is inversely proportional to the amount of dust shading the cell, whereas the performance loss for CS systems can be up to 14 times greater because the solar radiation has to pass twice through the soiled layer (Bellmann *et al.*, 2020). The schematic in Figure 1 illustrates the problem.

There is a complex relationship between meteorological comditions, site location, and reflector soiling (Pennetta *et al.*, 2016; Bouaddi, Ihlal, and Fernández-García, 2017). The performance of a CS plant depends on proper reflector cleaning strategies, which constitute a large part of operational and maintenance costs (Picotti *et al.*, 2020). This paper deals with soiling of solar reflectors in the vicinity of a ferromanganese smelter by industrial dust. The aim the study is to lessen the challenges involved in integrating CST technology into EIIs. The questions asked are:

- What are the soiling rates (reflectance losses) in the vicinity of a manganese smelter, and are they comparable to soiling rates found in arid regions?
- Does placement of the mirrors relative to the main dust source have an effect on soiling rates?
- Does industrial dust affect mirrors differently to naturally occurring dust?
- Can a heliostat field perform effectively in the vicinity of a manganese smelter?

The outcomes are intended to specifically benefit regions where a good solar and mineral resource base co-exist, and more generally any planned solar project in the vicinity of a 'point' dust source that can be considered separately from the surrounding 'area' source.

Data collection

A soiling study was carried out from February to November 2020, involving 32 reflectors grouped into four sets of eight reflectors, at different locations around the smelter. Various methods were used to characterize the dust in and around the plant, especially samples collected from the reflectors. Meteorological conditions were also recorded.

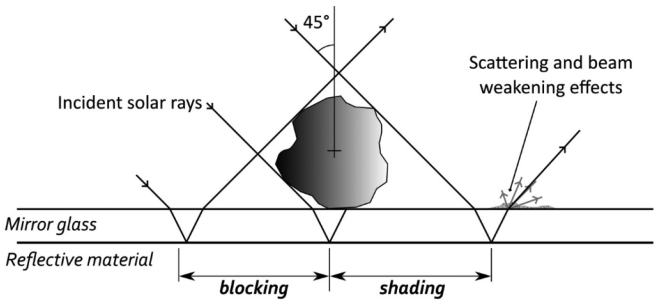

Figure 1—Illustration of the shading and blocking effect of dust particle on a solar reflector

Location

The investigation was conducted at Transalloys, a ferromanganese smelter in Emalahleni, Mpumalanga, South Africa. The plant is one of two ferromanganese producers in South Africa, with an annual production of around 165 000 t. The smelter is located in the industrial heart of South Africa (Figure 2), with numerous coal-fired power plants, coal mines, cement quarries, and ferrochrome smelters in the vicinity. These factors make Transalloys an ideal location at which to to investigate aspects of solar reflector soiling.

The following raw materials and process products are found at the plant.

- FeO_x—iron oxide dust produced during furnace tapping
- SiMn—silicomanganese dust produced during casting
- C—carbon dust from handling of high-carbon charcoal
- Baghouse dust—a mixture of FeO_x, SiMn, and C
- MnO_x—manganese ore dust resulting from ore handling
- SiO_2—quartz dust from raw materials handling
- Local red sand—dust generated by agricultural and other human activities, as well as natural processes.

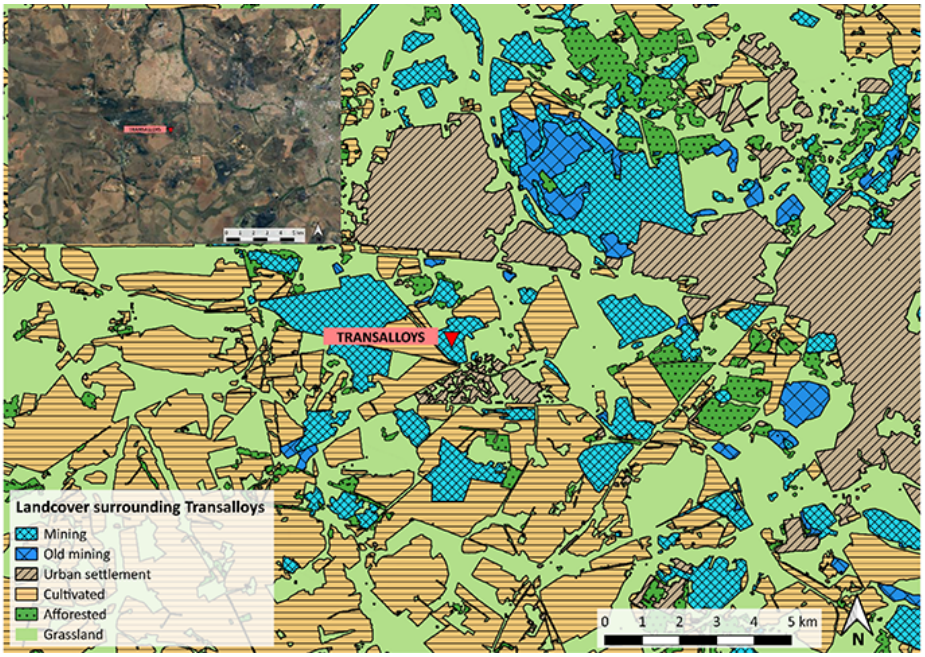

Figure 2—Land-use classifications of the area immediately surrounding the Transalloys ferromanganese smelter. Data from Lotter (2010) with Google Earth insert

Method

The aim of this study is to observe how soiling rates vary with reflector location and time of year. The reflectors were cleaned every 14 (±3) days by spraying with demineralized water using a hand-pump pressure sprayer, followed by wiping with a microfibre cloth to loosen the dust particles, and a final spray to remove loosened material. The aim was to clean the mirrors as well as possible, and not to test the effectiveness of cleaning.

Field soiling studies of solar reflectors are conducted using portable reflectometers, such as the ones compared by Fernández-García *et al.* (2017). Guidelines developed by a SolarPACES (Solar Power and Chemical Energy Systems) working group on reflectance measurement (Meyen *et al.*, 2018) were adhered to as far as is possible.

The measurement campaign procedures can be summarized as follows:

- Take reflectivity measurements of calibration mirror in the laboratory, and keep mirror in a safe place
- Install mirrors in field and take baseline reflectivity measurements of each mirror
- Let mirrors soil for 14 days
- Take reflectivity measurements of each mirror
- Wash mirrors after measuring reflectivity of soiled mirrors
- Take reflectivity measurements of cleaned mirrors
- Repeat steps 3 – 6 for the duration of the campaign

Wind speed and direction measurements were obtained using a standalone wind mast. All other meteorological parameters were gathered from a separate on-site weather station (Brooks *et al.*, 2015).

Equipment

The locations of the sampling sets, along with the wind mast location, are shown in Figure 3.

The wind mast consists of two 2-dimensional Gill Windsonic 1405-PK-100 SDI-12 ultrasonic anemometers, one at 4 m and one at 10 m height above the ground. The anemometers are capable of sampling the wind at 4 Hz and have a 0.01 m/s and a 1° resolution for wind speed and direction respectively. Figure 4 shows an image of the mast, located in an area with no significant obstructions.

The reflector samples were 5 mm thick, 200 mm by 400 mm, silvered second-surface low-iron glass with a protective vinyl coating applied on the back. The reflectors were installed 2 m above the ground and facing towards the smelter area, assumed to be the main dust source, with six reflectors at 60° elevation and two at 30° elevation. The reflectors were positioned in four-by-two arrays, each reflector spaced 2 m apart horizontally and diagonally, as shown in Figure 5. Dust deposition samplers were co-located with each set of reflectors to allow measurement of atmospheric dust characteristics.

The reflectivity measurements of the solar reflectors were made using a custom reflectometer developed by Griffith, Vhengani, and Maliage (2014) as an alternative to an off-the-shelf handheld reflectometer such as those described by Merrouni *et al.* (2017). This device offers the advantage of capturing images of the sampled reflector area, complementing the information obtained and allowing for qualitative visual inspection. The device and a schematic representation are shown in Figure 6.

A Nikon D5300 DSLR camera was attached to the custom lens and light system. The camera is built for professional use, with a very high signal-to-noise ratio. The sampling area is 17.7 mm by

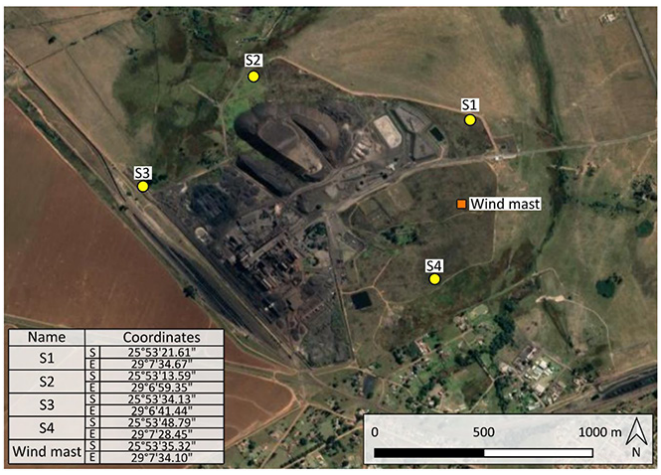

Figure 3—Reflector sampling sets and wind mast locations at the Transalloys site

Figure 4—Wind mast with two ultrasonic anemometers, one at 4 m and one at 10 m height

Figure 5—A reflector sampling set consisting of eight reflectors, six of which are elevated at 60° and two at 30°. Two dust fallout monitors can be seen in the background. The reflector set shown here is set four (S4). A ferrochrome smelter can be seen in the far background

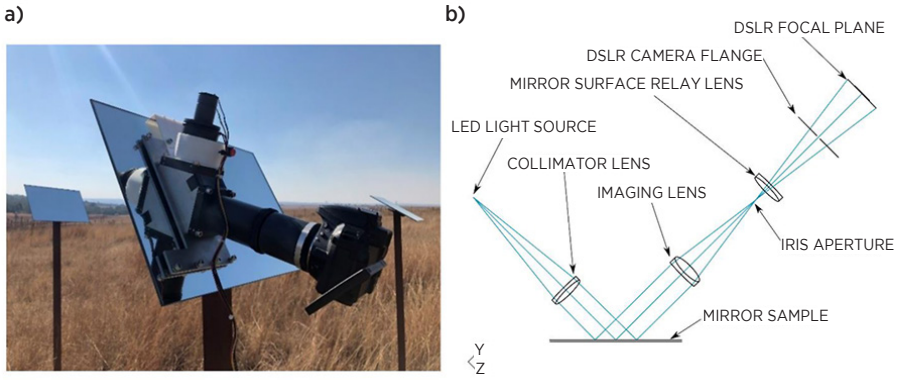

Figure 6—(a) Camera-based portable reflectometer on cleaned reflector, (b) schematic representation

16.8 mm, giving a linear field of view of approximately 300 mm². The reflectometer gives an incidence angle of $\theta_i = 45°$, and an acceptance aperture of $\phi = 15.7$ mrad. The angle of incidence is not considered to be near-normal. This is justifiable because a large proportion of heliostats in the concentrating solar field reflect at this range of incidence.

The camera-based reflectometer does not measure the incident light intensity required to determine reflectance. However, the specular reflectance can still be determined without knowing the incident light intensity. The detected beam intensities are a function of the same components, with different reflectance distribution functions. This allows the specular reflectance to be determined as the ratio of light intensity reflecting specularly from a soiled mirror to the intensity from a reference mirror, measured by the same receiving device. For convenience, this will be referred to simply as reflectance.

The method of calculating the reflectance for each mirror is described by Griffith, Vhengani, and Maliage, (2014). First, a dark image is taken to subtract from the illuminated image, cancelling out the camera sensor and background noise. Red-green-blue (RGB) mean channel pixel intensities (PIs) are then calculated for the corrected image, yielding PI_{RGB}. These two steps are repeated for a minimum of ten sampling spots, *Ns*, per mirror. The mirror mean is then calculated by

$$PI_{RGB,mean} = \frac{\sum PI_{RGB}}{N_s} \quad [1]$$

The mean PI for the mirror is then used to calculate the reflectance of the mirror as a fraction of the mean PI of a reference (calibration) mirror as follows:

$$mirror\_reflectance = \frac{PI_{RGB,mean;sampled}}{PI_{RGB,mean;reference}} \quad [2]$$

The reference mirror is kept in a clean laboratory environment. A representative reflectance is then calculated for each set of mirrors by

$$Mirror\_set\_reflectance = \frac{\sum mirror\_reflectance}{N_m} \quad [3]$$

where N_m represents the number of mirrors at the same elevation in the current set.

Results and discussion

Dispersed dust characterization

To establish whether the smelter is indeed the main dust source, both the total atmospheric dust and the dust soiling the reflectors were characterized. The deposited atmospheric dust (dustfall particles) was sampled after the extended March to May 2020 sampling period. The reflector soiling dust was sampled after the reflectance measurement campaign.

Particle size distributions (PSDs) for both samples were determined using a Malvern Mastersizer v3.63, which uses a laser diffraction measurement technique. Two separate composite samples, made up from the dust collected from the dust deposition buckets and the dust collected from the reflectors, were analysed. The PSDs for both composite samples are shown in Figure 7.

The PSD curves indicate that the dust present in the atmosphere has a much wider size range than the dust found on the reflectors. It was observed that particles larger than 100 µm tend to fall off the mirror, and for the most part are transported only a limited distance from the dust source, as shown by the count peak of the atmospheric dust PSD being below 100 µm. The mean dust particle size found on the reflectors was 35.5 µm, with 50% of the sample being less than 31.1 µm, and 90% smaller than 98 µm.

The dust morphology was assessed by high-resolution imaging using scanning electron microscopy (SEM) at different magnifications, as shown in Figure 8. The secondary electron detector of a Joel JSM 6360LV instrument was used for this purpose.

The SEM images show agglomerates of small particles that formed during storage, and which do not represent the state the dust was collected in. The particle shapes become more visible at the largest magnification. Some rough edges are visible, but not enough for the particles to be called jagged or abrasive.

Quantitative analysis was conducted using a Thermo Noran energy dispersive spectroscopy (EDS) instrument. A representative spectrum of the reflector dust is shown in Figure 9.

The data in Figure 9 is summarized in Table I. The three dominant elements were Si (23.46%), Al (15.15%), and Fe (8.16%).

The crystalline phases present in the sample were identified by X-ray diffraction (XRD) analysis using a Bruker D8 diffractometer with a Fe-filtered Co-K radiation source and a point detector. The Bruker EVA software was used with a reference intensity ratio method to perform phase matching. The phase matching results should thus be considered low-confidence and semi-quantitative only. Phase matching revealed that silica-related phases were dominant:

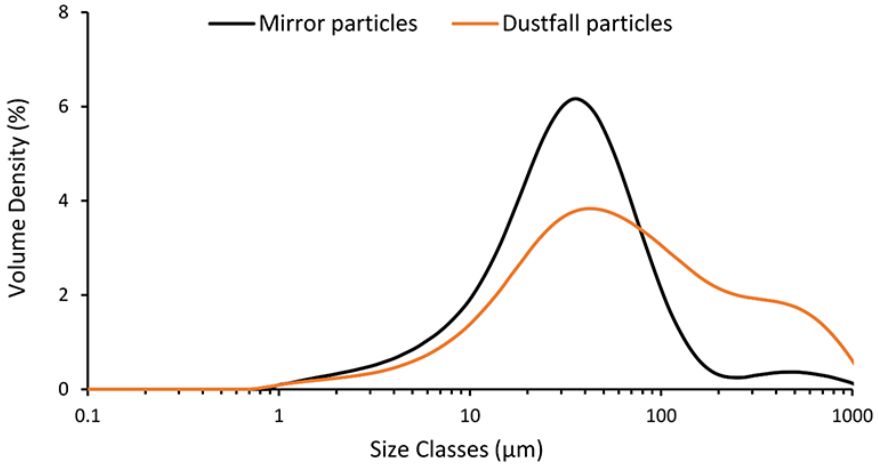

Figure 7—PSDs of dust collected from dustfall monitors and from reflector samples

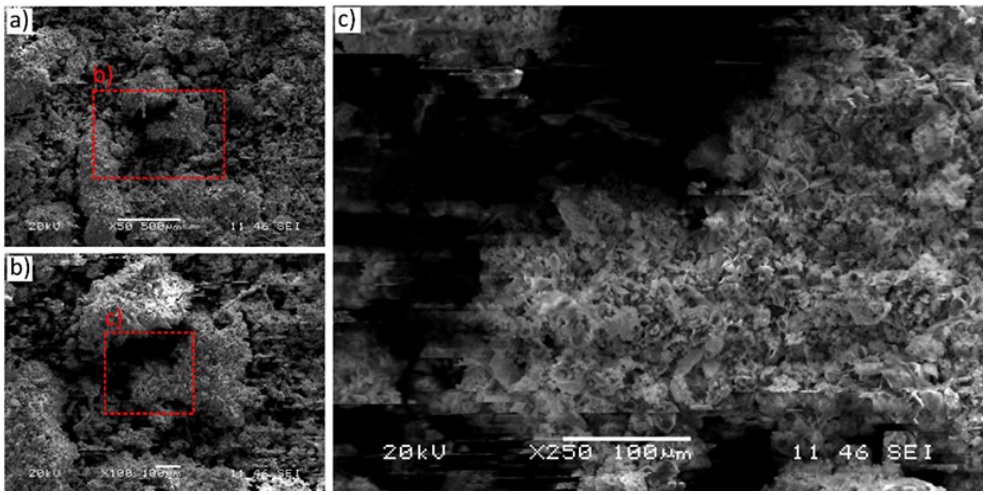

Figure 8—Secondary SEM images of dust samples collected from reflectors. (a) 50× magnification, (b) 100× magnification, (c) 250× magnification

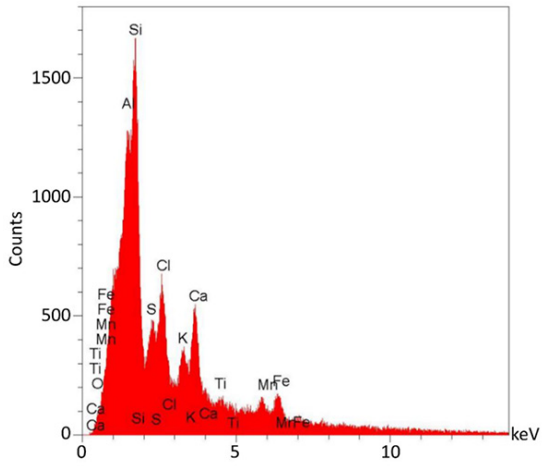

Figure 9—Representative EDS spectrum of reflector dust

- SiO_2 - silica
- Fe_2SiO_4 – iron silicate
- $Al_2O_3.SiO_2$ - kyanite
- $Al_9Fe_2Si_2$ – ferrosilicon aluminium

Table I

Summary of chemical composition of reflector dust sample, (wt. %)

Element	Si	Al	Fe	S	O	Mn
Sample	23.5	15.2	8.2	7.7	7.5	5.8

The oxide phases are common in sand as well as ores. Routine XRD analysis detects above-trace levels of alumina (Al_2O_3) in coals, ores, and slag at the smelter site.These materials are the most likely source of the aluminium oxide-related phases but not the silica. The alumina content in the coal is typically approximately 1%, with 4–5% in the manganese ores and 3–6% in the slags. Although the alumina concentration in the raw coal is considered low, alumina constitutes 3–7% of the 15% ash content of the reacted coal. The silica phase could originate either from the raw silica (quartz) stockpiles or from sand at the site; probably a combination of both. The most common phase (SiO_2) is also the least dense(2.20 g/cm^3), suggesting that less dense phases are more likely to disperse further from their source than denser phases. The other common phases found, including the aluminium phases, probably originate from fugitive furnace dust or (more likely) from the baghouse.

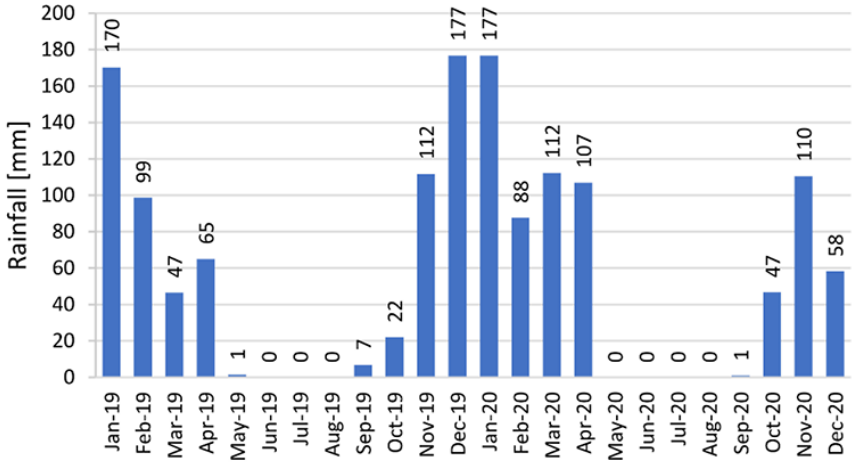

Figure 10—Rainfall measured at Transalloys site from January 2019 to December 2020

As the slag heaps are formed by dumping of liquid and solidified slag, slag particles are likely to be larger than dust and ore particles. Slags are also handled less than raw materials and it therefore makes sense that dust from the slag products does not seem to contribute significantly to mirror soiling.

Atmospheric conditions

Rainfall data for two full seasons is shown in Figure 10. The dry winter season (June-August) coincides with a decrease in reflectance and rise in soiling trends (Figures 12 and 13, respectively).

Wind mast data is displayed in Figure 11 in the form of wind roses. The data is for seven two-week periods during the dry season when increased loss of reflectance was observed (June to September), chosen. to coincide with reflectance sampling dates. The dominant wind direction during this period was from the southwest.

Figure 11 reveals that the wind blows predominantly from the north-northeast (NNE) or the south-southwest (SSW) directions. A peak wind is defined here as a wind speed equal to or above 6 m/s at 10 m above the ground, which occurred roughly 18% of the time during the study period.

Reflectance measurements

The results from the reflectance measurement campaign are presented in Figure 12. Only results from the reflectors at 60° are shown here as soiling for the reflectors at 30° follows similar trends, except with more intense soiling as expected. The maximum measurement uncertainty is 3.2%, with an average uncertainty of 1.3%, which is acceptable. The standard deviation from the averaged reflectance of each reflector set is used as a proxy for uncertainty.

The reflectance of all mirrors starts off at 1.0 and decreases until the reflectors are cleaned. The goal was to take samples every 14 days, but this was not always possible. Notably, the second soiling period (6 March to 13 May) was 68 days, corresponding to a nationwide lockdown due to the COVID-19 pandemic. The reflectance loss during this period averaged 32.7% across the four reflector sets, which is markedly less than the averaged losses of 32.6% experienced over the consecutive 14-day sampling periods during the dry season (26 June to 22 September). These reflectance losses, while high, are not uncommon in arid regions. The differences in soiling for sampling sets S1-to-S4 are also greater in the dry season.

A comparison of the rainfall data (Figure 10) with the soiling results (Figure 12) shows a decrease in reflectance losses with the first rains in the region around the end of September. The rain reduces the levels of atmospheric dust, thereby decreasing the potential for soiling, and washes dust collected off the reflectors.

The smelter shutdown in August does not appear to significantly impact measured reflectance on any of the sampling sets. This seems to contradict the conclusion drawn from dust characterization, that furnace emissions are a major dust source as well as those reached by Davourie *et al.* (2017), who cited furnace processes and stack emissions as contributing a large proportion of total plant dust emissions. These apparently disparate conclusions can be reconciled if we consider that a large fraction of the furnace ground-level and stack emissions settles out near the origins, resulting in a dust 'reservoir' everywhere in close proximity to the major emission sources. During a shutdown, dust will still be dispersed much as usual from these areas. This implies that dust emission control at source will be effective only if the existing dust 'reservoirs' are also suppressed.

The mean daily reflectance loss (MDRL) data, or rate of change in reflectance for that period, calculated from the data presented in Figure 12, is in Figure 13. The MDRL is a better way of interpreting the data because it accounts for time, making it easier to identify the worst soiling periods.

Analysis of wind and soiling data

Although background dust concentrations and levels of activity on the plant play a role, the major comntributor to soiling is assumed to be the plant area, based on the dust characterization results.

A first inspection of Figure 13 shows that reflector set S3 consistently experienced higher levels of soiling than the other three sets during the dry season. The marked changes from one period to the next show that there are factors that influence soiling apart from proximity, but for S3 proximity to source clearly outweighs these other factors. The worst soiling is observed during the height of the dry season àt the beginning of August when the most dust is present in the atmosphere. S3 experienced a significantly higher soiling rate with an MDRL of 0.043, in comparison to the rates at S1 and S2 with MDRLs of 0.028 and 0.026 respectively. The weakest winds of the entire sampling period occurred during this time.

Upon closer inspection of the data some interesting trends emerge. During periods A and B (11–26 June and 26 June–8 July)

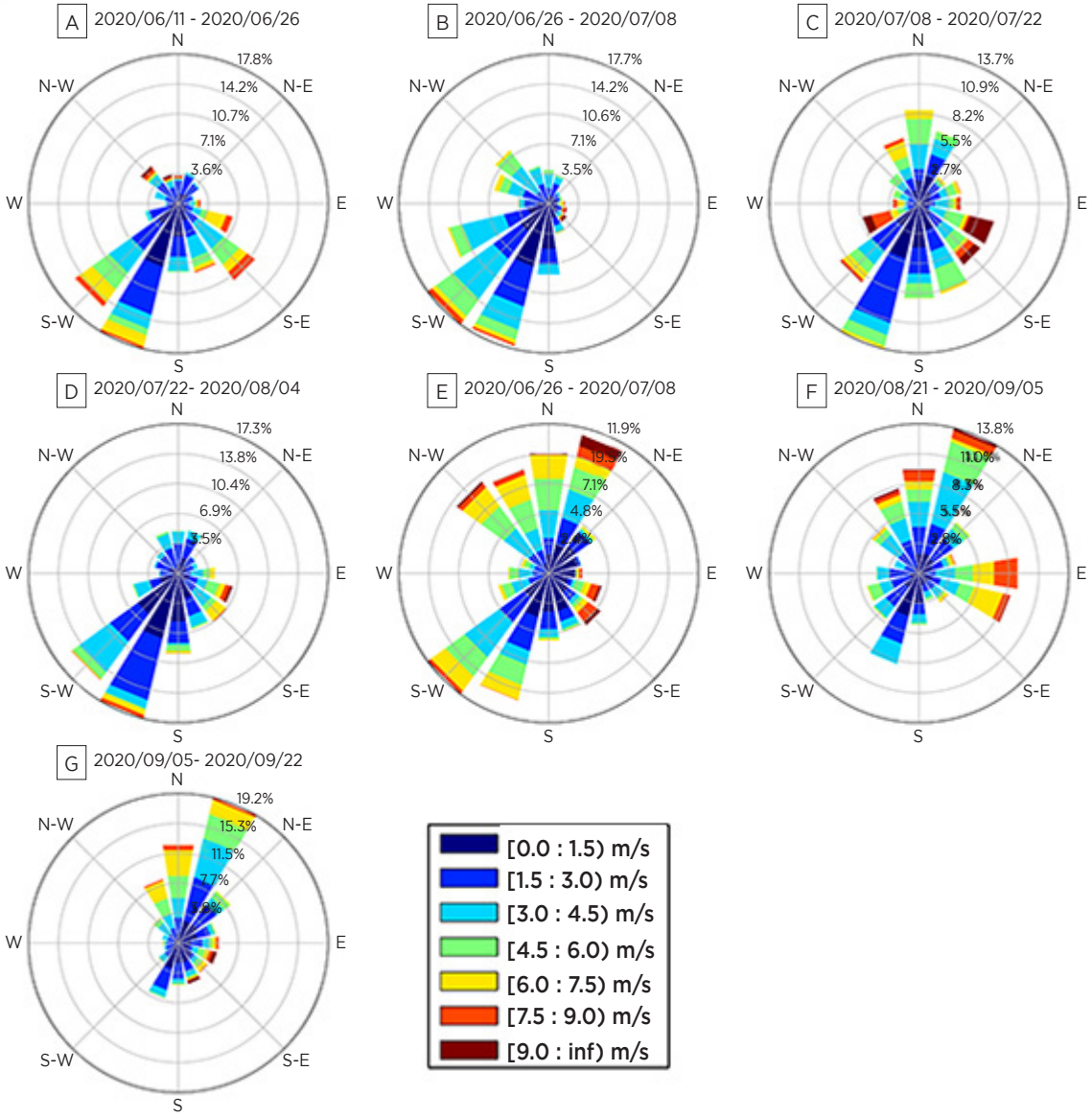

Figure 11—Wind data corresponding to the reflectance sampling periods. Data averaged over 10-minute intervals, measured at 10 m height above ground, from 11 June to 1 October 2020

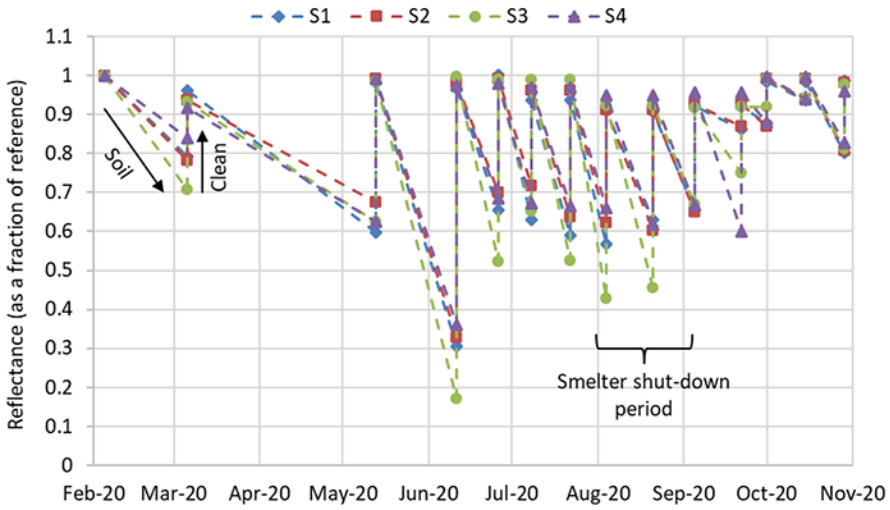

Figure 12—Reflectance of the 60° elevation reflectors for all four sampling sets (S1 to S4) from 5 February to 29 October 2020.

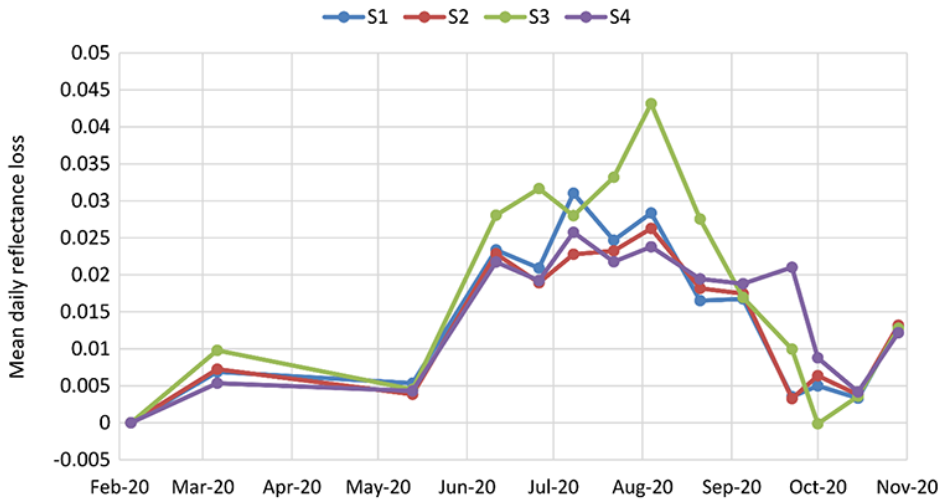

Figure 13—MDRL of the 60° elevation reflectors for all four sampling sets (S1 to S4), from 5 February - to 29 October 2020

the wind data appears to be very similar, yet the soiling rates are different. The highest soiling rate observed for period A occurs at S3 with an MDRL of 0.032, and the second highest at S1 with an MDRL of 0.021, a significant difference. In period B the highest soiling rate is for S1 with an MDRL of 0.031, and the second highest at S3 with an MDRL of 0.028. During both periods the winds were predominantly SW and SSW, except for the SE tertiary wind reaching peak speeds for a short while in period A.

During period C the highest soiling rate was at S3 with an MDRL of 0.033, and the second highest at S1 with an MDRL of 0.025. The winds were predominantly SSW, with only short-duration peak winds from other directions.

There are clear changes in the MDRL patterns for the different reflector sets for periods E to G. A general decrease in soiling rates is noted as the winds speeds increase and with the first rains falling towards the end of September. The MDRLs are similar for all reflector sets in period F, as a result of the variability in wind direction. Period F signifies a turning point coinciding with the change of season, with S3 no longer consistently experiencing the worst soiling. The winds were predominantly NNE/N in period G, causing S4 to experience a significantly higher soiling rate than the other sets, with an MDRL of 0.021.

The performance of the different reflector sets during the dry season is simmarized in Table II. The averaged MDRLs are listed alongside a simple scoring system, with one point assigned to the set with the highest MDRL during a particular period and four points to the lowest MDRL.

This analysis leads to the conclusion that although the soiling intensity is determined mainly by the predominant wind direction, shorter duration peak winds can disproportionately influence soiling rates. Thus merely considering predominant wind directions might not be adequate if there is a clear point source of dust close to a planned CS site. The data also reveals that S3 is poorly situated, experiencing much higher soiling rates than the other three sampling locations throughout the dry season. S4 and S1 performed similarly, with averaged MDRLs of 0.0214 and 0.0203 respectively, and S2 perform the best with an averaged MDRL of 0.0186, 13.1% lower than S4.

Dependence of soiling rate on reflector location

Figure 14 shows the relative contributions of different parts of the plamt to dust generation, based on the dust characterization

Table II

Reflector set performance scoring for the considered dry season, periods A-to-G, with higher being better

Reflector set	Averaged MDRL	Score
S2	0.0186	23
S1	0.0203	18
S4	0.0214	18
S3	0.0272	11

study, observations made throughout the campaign, and informal discussions with staff at the site.

The three different source strength categorues are:

- Major dust sources—dust from the baghouse endpoints, furnace emissions, metal tapping and casting zones, all contributing to the hypothesised 'dust reservoir'
- Intermediate dust sources—raw materials handling and screening
- Minor dust sources—slag heaps and general smelter area.

A cause-and-effect relationship emerges from the soiling data and the wind direction data for the same sampling periods. This relationship is most apparent during the dry season. Figure 15 shows image data from two sampling sets, one pair of images acquired during the dry season and the other when the rains have started falling.

Figure 15 clearly shows the difference in soiling between the dry and wet seasons. Sites S1 and S4 were chosen to illustrate this because they are only about 500 m apart, and yet there is a clear difference in the amount of dust seen on the surfaces regardless of the season. The images correspond to period E in Figure 11, with predominant and peak winds blowing from the NW or NNE sending more dust in the direction of S4.

Conclusions

An average reflectance loss of 32.6% for all for sampling sets was observed for the 14-day sampling periods during the dry season. If, however, the poorly sited reflector set S3 is excluded, an average loss of 22.6% is obtained.

It was found that the position of the reflector sets in relation to the plant area, together with the wind direction, determines

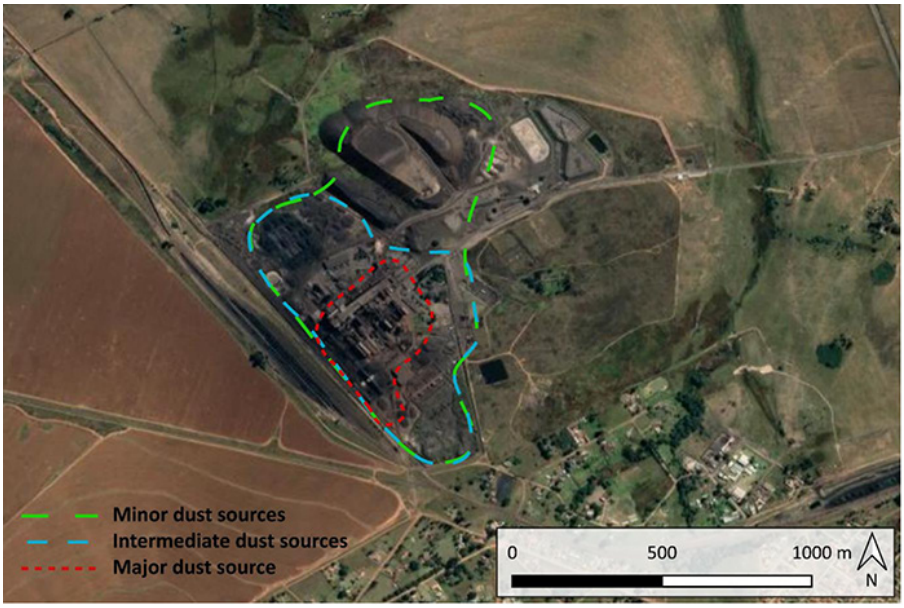

Figure 14—Relative contributions of different parts of the plamt to dust generation

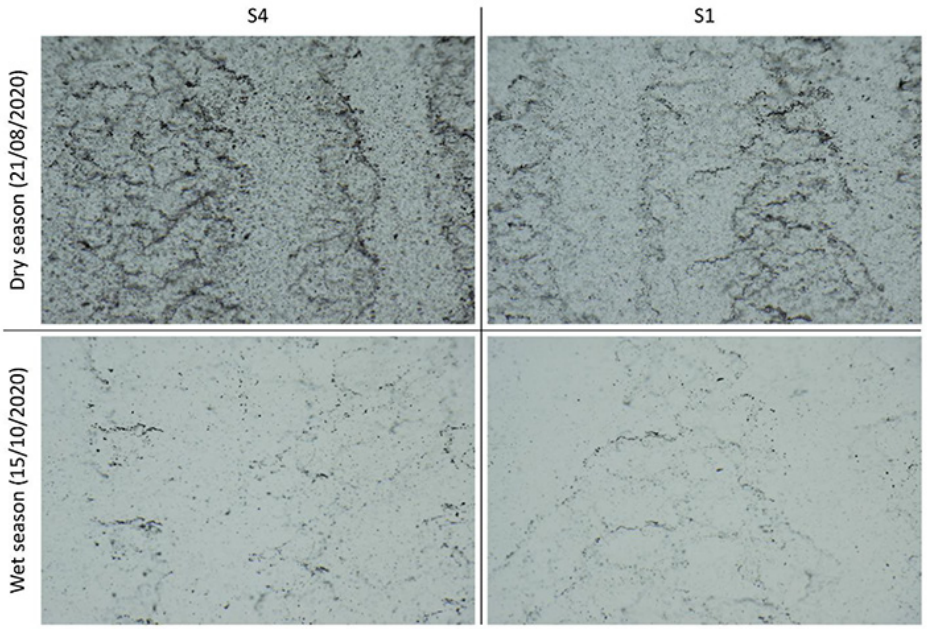

Figure 15—Captured image data from the reflectometer for a reflector in S1 and S4, each for the dry and wet season

the intensity of soiling. A 44.8% difference in MDRL (mean daily reflectance loss) for the worst period (in terms of soiling) was observed for two reflector sets in different locations. It was also found that peak winds (> 6 m/s) can disproportionately impact where the most soiling occurs, even if these are not from the dominant wind direction. The peak soiling period coincided with the weakest winds, leading to the conclusion that 'wind washing' does help to limit soiling during dry dusty periods.

The dust characterization study revealed that 90% of the particles found on the reflector surfaces were smaller than 98 µm, with 50% less than 31.5 µm. The main dust elements were Si, Al, Fe, S, O, and Mn. The phases identified were SiO_2, Fe_2SiO_4, Al_2O_3. SiO_2, and $Al_9Fe_2Si_2$, none of which are expected to have particularly adverse effects on the reflectors' useful lifetime. SEM micrography also revealed that the particle morphology is not particularly abrasive and the dust is therefore not expected to pose a serious risk of increased mechanical wear on a reflector surface when washing. The project did not last long enough to draw conclusion regarding reflector degradation resulting from the environment over lifetime use.

The results of the study point to a number of methods for preventing and mitigating solar reflector soiling. A minor difference in reflector location relative to the dust source resulted in a 13.1% lower soiling rate. At the reflector set with the lowest averaged MDRLduring the dry season, it is conceivable that by utilizing other well-known interventions such as anti-soiling coatings, an

acceptable soiling rate coukd be achieved. It is recommended that any soiling mitigation technique, including choosing an appropriate location relative to source, should be optimized to have the greatest effect during the season when the most severe soiling is expected.

Acknowledgements

This paper is published by permission of the University of Pretoria, the University of Stellenbosch, Transalloys, and Mintek. This project has received funding from the European Union's Horizon 2020 research and innovation programme under grant agreement no. 820561. The authors would like to thank the EU Horizon programme for its continued support of research and development projects working towards a sustainable future. Further gratitude is expressed to the CSIR for the use of their reflectometer, and to the Southern African Universities Radiometric Network (SAURAN) for providing research-quality meteorological data. Melanie Smit (Mintek) is also thanked for her contribution to the dispersed dust characterization work.

References

Bellmann, P.,Wolfertstetter, F., Conceição, and Silva, H.G. 2020. Comparative modeling of optical soiling losses for CSP and PV energy systems. *Solar Energy*, vol. 197. pp. 229–237. doi: 10.1016/j.solener.2019.12.045

Bouaddi, S., Ihlal, A., and Fernández-García, A. 2017. Comparative analysis of soiling of CSP mirror materials in arid zones. *Renewable Energy*, vol. 101. pp. 437–449. doi: 10.1016/j.renene.2016.08.067

Brooks, M.J. du Clou, S., van Niekerk, W.L., Gauché, P., Leonard, C., Mouzouris, M.J., Meyer, R., van der Westhuizen, N., van Dyk, E.E., and Vorster, F.J. 2015. SAURAN: A new resource for solar radiometric data in Southern Africa. *Journal of Energy in Southern Africa*, vol. 26.pp. 2–10.

Costa, S.C.S., Diniz, A.S.A.C., and Kazmerski, L.L. 2016. Dust and soiling issues and impacts relating to solar energy systems: Literature review update for 2012-2015. *Renewable and Sustainable Energy Reviews* [preprint]. doi: 10.1016/j.rser.2016.04.059

Costa, S.C.S., Diniz, A.S.A.C., and Kazmerski, L.L. 2018. Solar energy dust and soiling R&D progress: Literature review update for 2016. *Renewable and Sustainable Energy Reviews*, vol. 82. pp. 2504–2536. doi:10.1016/j.rser.2017.09.015

Davourie, J., Westfall, L., Ali, M., and McGough, D. 2017. Evaluation of particulate matter emissions from manganese alloy production using life-cycle assessment. *NeuroToxicology*, vol. 58. pp. 180–186. doi: 10.1016/j.neuro.2016.09.015

Ebert, M., Amsbeck, L., Buck, R., Rheinländer, J., Schlögl-Knothe, B., Schmitz, S., Sibum, M., Stadler, H., and Uhlig, R. 2018. First on-sun tests of a centrifugal particle receiver system. *Proceedings of the ASME 2018 12th International Conference on Energy Sustainability collocated with the ASME 2018 Power Conference and the ASME 2018 Nuclear Forum*, Lake Buena Vista, FL.. American Society of Mechanical Engineers. p. V001T11A002. doi: 10.1115/ES2018-7166

Fernández-García, A., Sutter, F., Martínez-Arcos, L., Sansom, C., Wolfertstetter, F, and Delord, C. 2017. Equipment and methods for measuring reflectance of concentrating solar reflector materials. *Solar Energy Materials and Solar Cells*, vol. 167. pp. 28–52. doi: 10.1016/J.SOLMAT.2017.03.036

Griffith, D.J., Vhengani, L., and Maliage, M. 2014. Measurements of mirror soiling at a candidate CSP Site. *Energy Procedia*, vol. 49. pp. 1371–1378. doi: 10.1016/j.egypro.2014.03.146

Hockaday, L., McKechnie, T., von Puttkamer, M.N., and Lubkoll, M. 2020. The impact of solar resource characteristics on solar thermal pre-heating of manganese ores. *Proceedings of Energy Technology 2020: Recycling, Carbon Dioxide Management, and Other Technologies*. Chen, X., Zhong, Y., Zhang, L., Howarter, J.A., Baba, A.A., Wang, C., Sun, Z., Zhang, M., Olivetti, E., Luo, A., and Powell, A. (eds). Springer, Cham. pp. 3–13. doi: 10.1007/978-3-030-36830-2_1

Hund, K. , la Porta, D., Fabregas, T.P., Laing, T., and Drexhage, J. 2020. Minerals for Climate Action: The Mineral Intensity of the Clean Energy Transition. World Bank, Washington.

IPCC. 2014. Contribution of Working Group III to the Fifth Assessment Report of the Intergovernmental Panel on Climate Change. Cambridge University Press. 1454 pp.

IRENA. 2021. Renewable Power Generation Costs in 2020. International Renewable Energy Agency, Abu Dhabi.

Kazmerski, L.L., Diniz, A.S.A.C., and Costa, S.C.S. 2020. Dust in the wind: An historical timeline of soiling R&D for solar technologies. *Proceedings of the ISES Solar World Congress 2019 and IEA SHC International Conference on Solar Heating and Cooling for Buildings and Industry 2019*. doi: 10.18086/swc.2019.54.01

Lotter, M.C. 2010. MBSP Landcover 2010 [Vector] 2010. Mpumalanga Tourism and Parks Agency. http://bgis.sanbi.org/SpatialDataset (accessed 15 September 2020).

Mckechnie, T., McGregor, C., and Venter, G. 2020. Concentrating solar thermal process heat for manganese ferroalloy production: Plant modelling and thermal energy storage dispatch optimization. *Proceedings of the ASME 2020 14th International Conference on Energy Sustainability*. American Society of Mechanical Engineers. p. V001T14A001. doi: 10.1115/ES2020-1635

Mehos, M., Price, H., Cable, R., Keamey, D., Kelly, B., Kolb, G., and Morse, F. 2020. Concentrating solar power best practices study. *Technical Report* NREL/TP-5500-75763. National Renewable Energy Laboratory. wahington. 269 pp. https://www.nrel.gov/docs/fy20osti/75763.pdf

Merrouni, A.A. , Mezrhab, A., Ghennioui, A., and Naimi, Z. 2017. Measurement, comparison and monitoring of solar mirror's specular reflectivity using two different reflectometers. *Energy Procedia*, vol. 119. pp. 433–445. doi: 10.1016/J.EGYPRO.2017.07.045

Meyen, S., Monteccji, M., Kennedy, C., Zhu, G., Gray, M., Crawford, J., Jiemer, S., Platzer, W., Heimsath, A., O'Neill, M., Ziegler, S., Brändle, S., and Fernandez, A. 2018. Parameters and method to evaluate the solar reflectance properties of reflector materials for concentrating solar power technology. SolarPACES. https://www.solarpaces.org/wp-content/uploads/Document-1_SolarPACES_Reflectance-Guideline_V3.1.pdf

Pennetta, S., Yu,S., Borghesani, P., Cholette, M., and Barry, J. 2016. An investigation on factors influencing dust accumulation on CSP mirrors. *SOLARPACES 2015: Proceedings of the International Conference on Concentrating Solar Power and Chemical Energy Systems*, Cape Town, South Africa. p. 070024. doi: 10.1063/1.4949171

Picotti, G., Moretti, L., Cholette, M.E., Binotti, M., Simonetti, R., Martelli, E., Steinberg, T.A., and Manzolini, G. 2020. Optimization of cleaning strategies for heliostat fields in solar tower plants. *Solar Energy*, vol. 204. pp. 501–514. doi: 10.1016/j.solener.2020.04.032

Reichart, M., Puttkamer, M.N., Buck, R., and Pitz-Paal, R. 2021. Numerical assessment of packing structures for gas-particle trickle flow heat exchanger for application in CSP plants. *ASME 2021: Proceedings of the 15th International Conference on Energy Sustainability*. American Society of Mechanical Engineers. https://doi.org/10.1115/ES2021-62746

Sambo, S.N., Hockaday, C.S.A., and Seodigeng, T. 2020. The development of a heat and mass transfer model for a shaft kiln to preheat manganese ore with hot air, model development methodology. *Proceedings of the 11th International Symposium on High-Temperature Metallurgical Processing*. Peng, Z., Hwang, J-Y., Downey, J.P., Gregurek, D., Zhao, B., Yücel, G., Keskinkilic, E., Jiang, T., White, J.F., and Mahmoud, M.M. (eds). Springer, Cham. pp. 43–53. doi: 10.1007/978-3-030-36540-0_5

Weiss, W. and Spörk-Dür, M. 2021. Solar Heat Worldwide - Edition 2021. AEE - Institute for Sustainable Technologies, Gleisdorf, Austria. ◆